Crystal Structure Revision and Identification of Li^+-Ion Migration Pathways in the Garnet-like $Li_5La_3M_2O_{12}$ (M = Nb, Ta) Oxides

Venkataraman Thangadurai,*,† Stefan Adams,*,‡ and Werner Weppner*,†

Chair for Sensors and Solid State Ionics, Faculty of Engineering, University of Kiel, Kaiserstr. 2, D-24143 Kiel, Germany, and GZG Geoscience Center, Department of Crystallography, Universität Göttingen, Goldschmidtstr. 1, D-37077 Göttingen, Germany

Received December 15, 2003. Revised Manuscript Received May 24, 2004

Bond valence sums for the ion positions in single-crystal structure data of the garnet-like fast lithium ion conductors $Li_5La_3M_2O_{12}$ (M = Nb, Ta) exhibit unusually large deviations from the ideal valences. The root-mean-square bond valence mismatch (commonly termed "global instability index" GII) and the chemical plausibility of the structure model can be significantly improved by optimizing the light atoms (oxygen and lithium) positions using a bond valence mismatch minimization procedure in the previously suggested space group $I2_13$ or its centrosymmetric counterpart $Ia\bar{3}$. Possible pathways for lithium ion migration in $Li_5La_3M_2O_{12}$ are identified by a bond valence analysis. Li-bond valence mismatch isosurface models for Li^+-ion transport pathways are found to be nearly the same in both compounds $Li_5La_3Nb_2O_{12}$ and $Li_5La_3Ta_2O_{12}$. The characteristic feature of the three-dimensional Li^+-ion pathway network is a nonplanar square of partially occupied Li sites.

1. Introduction

The development of solid lithium ion electrolytes with suitable functional properties has drawn much attention due to their various possible electrochemical applications that include solid-state batteries, sensors, and electrochromic displays.[1,2] In this regard, several lithium-containing metal oxides have been explored in recent years. Among the most well-known solid lithium ion conductors,[3−6] the perovskite (ABO_3)-type lithium lanthanum titanate $Li_{3x}La_{(2/3)-x}\square_{(1/3)-2x}TiO_3$ ($\sim 0.04 < x < \sim 0.16$) (LLT) exhibits the highest bulk lithium ion conductivity.[5,6] For $x \approx 0.1$ a bulk (grain interior, σ_{bulk}) conductivity of about 1×10^{-3} S/cm is observed at room temperature, which is comparable to that of currently used polymer/liquid electrolytes in the lithium ion battery technology. However, LLT is not favorable to be employed as an electrolyte in the high-energy density all-solid-state batteries using a Li metal anode since LLT is not stable in direct contact with elemental lithium and undergoes fast Li insertion with the consequent reduction of Ti^{4+} to Ti^{3+}, resulting in high electronic conductivity. On the other hand, the use of LLT as an electrode material is also limited because of the small lithium uptake.[7,8]

Until now, a high Li^+-ion conductivity together with chemical stability (against electrode materials such as metallic lithium) and electrochemical stability have been reported for a few crystalline/amorphous compounds containing polyanions such as SiO_4^{4-} or PO_4^{3-}, for example, Li_4SiO_4 and Li_3PO_4 structure-related materials.[1,3,9] Recently, we have reported fast lithium ion conductivity[10] in the lithium-containing metal oxides with the nominal chemical composition $Li_5La_3M_2O_{12}$ (M = Nb, Ta), which are structurally related to the garnet structure. These oxides had been identified in investigations of the ternary phase diagram $La_2O_3-M_2O_5-Li_2O$.[11,12] Both $Li_5La_3Nb_2O_{12}$ and $Li_5La_3Ta_2O_{12}$ exhibit

* All authors may receive correspondence. E-mail, sadams@gwdg.de; phone, +49-551/39 3898; fax, +49-551/39 9521 (S. Adams). E-mail, vt@tf.uni-kiel.de (V. Thangadurai). E-mail, ww@tf.uni-kiel.de (W. Weppner); phone, +49-431/880 6210; fax, +49-431/880 6203.

† University of Kiel.

‡ Universität Göttingen.

(1) Robertson, A. D.; West, A. R.; Ritchie, A. G. *Solid State Ionics* **1997**, *104*, 1.

(2) Adachi, G. A.; Imanaka, N.; Aono, H. *Adv. Mater.* **1996**, *8*, 127.

(3) (a) Irvine, J. T. S.; West, A. R. in *High Conductivity Ionic Conductors, Recent Trends and Application*; Takahashi, T., Ed.; World Scientific: Singapore, 1989; p 201. (b) Kudo, T.; Fueki, K. *Solid State Ionics*; VCH Publishers: Weinheim, Germany, 1990. (c) Thangadurai, V.; Weppner, W. *Ionics* **2002**, *8*, 281.

(4) Birke, P.; Weppner, W. In *Handbook of Battery Materials*; Besenhard, J. O., Ed.; Wiley-VCH Publishers: Weinheim, Germany, 1999; p 525.

(5) (a) Belous, A. G.; Novitskaya, G. N.; Polyanetskaya, S. V.; Gornikov, Yu. I. *Inorg. Mater.* **1987**, *23*, 412. (b) Inaguma, Y.; Liquan, C.; Itoh, M.; Nakamura, T.; Uchida, T.; Ikuta, H.; Wakihara, W. *Solid State Commun.* **1993**, *86*, 689. (c) Inaguma, Y.; Chen, L.; Itoh, M.; Nakamuara, T. *Solid State Ionics* **1994**, *70/71*, 196. (d) Itoh, M.; Inaguma, Y.; Jung, N. H.; Nakamuara, T. *Solid State Ionics* **1994**, *70/71*, 203. (e) Fourquet, J. L.; Duroy, H.; Crosnier-Lopez, M. P. *J. Solid State Chem.* **1996**, *127*, 283. (f) Thangadurai, V.; Weppner, W. *Ionics* **2000**, *6*, 70.

(6) Stramare, S.; Thangadurai, V.; Weppner, W. *Chem. Mater.* **2003**, *15*, 3974.

(7) (a) Bohnke, O.; Bohnke, C.; Fourquet, J. L. *Solid State Ionics* **1996**, *91*, 21. (b) Birke, P.; Scharner, S.; Huggins, R. A.; Weppner, W. *J. Electrochem. Soc.* **1997**, *144*, L167.

(8) Chen, C. H.; Amine, K. *Solid State Ionics*, **2001**, *144*, 51.

(9) (a) Neudecker, B. J.; Weppner, W. *J. Electrochem. Soc.* **1996**, *143*, 2198. (b) Yu, X.; Bates, J. B.; Jellison, G. E.; Hart, F. X. *J. Electrochem. Soc.* **1997**, *144*, 524.

(10) Thangadurai, V.; Kaack, H.; Weppner, W. *J. Am. Ceram. Soc.* **2003**, *86*, 437.

(11) Mazza, D. *Mater. Lett.* **1988**, *7*, 205.

(12) Hyooma, H.; Hayashi, K. *Mater. Res. Bull.* **1988**, *23*, 1399.

10.1021/cm031176d CCC: $27.50
Published on Web 07/15/2004

a similar order of magnitude of bulk lithium ion conductivity of $\sim 10^{-6}$ S/cm at 25 °C with activation energies of 0.43 and 0.56 eV, respectively.[10] Among the two compounds, the Ta compound $Li_5La_3Ta_2O_{12}$ is of particular interest as an electrolyte material for solid-state batteries due to its stability against reaction with molten Li. These compounds are the first examples for fast lithium ion conductivity within a garnet-like structure and thereby open a new field for conductivity optimization by structural modifications.

Garnets constitute a large family of orthosilicate minerals with the general formula $A_3^{II}B_2^{III}(SiO_4)_3$ (A = Ca, Mg, Fe; B = Al, Cr, Fe), in which A and B cations are respectively 8- and 6-coordinated by oxygen. Since the garnet structure contains 8-, 6-, and 4-fold coordinated cation sites, a large variety of cations in different valence states, for example, alkali, alkaline earth, rare earth, and transition metal ions can be accommodated by replacing either A or B or Si sites.[13,14] Well-known non-silicate garnet structures include, for example, the technologically relevant metal oxides $A_3M_2(MO_4)_3$ (A = Y, Gd; M = Fe, Al, Ga) that crystallize in the aristotype garnet space group $Ia\bar{3}d$. Cation ordering in garnets is known to lead to phases with reduced symmetries.

The structure of $Li_5La_3M_2O_{12}$ (M = Nb, Ta) had been determined in 1988 from powder XRD data by Mazza[11] as well as from single-crystal data by Hyooma and Hayashi.[12] Mazza described the structure as being closely related to the garnet structure (SG $Ia\bar{3}d$ (No. 230), $a = 12.8$ Å, La^{3+} on the A^{II} site $^1/_8$, 0, $^1/_4$; Nb^{5+} or Ta^{5+} on the B^{III} site 0, 0, 0; three of the Li^+ on the tetrahedrally coordinated Si^{IV} site $^3/_8$, 0, $^1/_4$) with the exception that two additional Li^+ per formula unit should fully occupy the octahedrally coordinated site $^1/_8$, $^1/_8$, $^1/_8$ that is vacant in the ideal garnet structure. In this structure model, only the oxygen site contains refinable atomic coordinates (three refinable atomic coordinates).

Hyooma and Hayashi,[12] however, proposed a lower symmetry non-centrosymmetric space group $I2_13$ (No. 199). In comparison to the aristotype $Ia\bar{3}d$, this model with 20 refinable atomic coordinates suggests not only splitting each cation site into 2 crystallographically independent sites (and 4 independent sites for the oxygen atoms) but also turning the special position for the La^{3+} into two refinable sites of the type x, 0, $^1/_4$. The higher structural flexibility of the lower symmetry model becomes also evident from the reported Li distribution onto two 24-fold general sites with octahedral oxide coordinations. The octahedron around Li(1) (occupancy $^2/_3$) is reported to be more distorted than that around the fully occupied Li(2) site.[12] It appears tempting to attribute the observed high Li^+-ion conductivity to the high concentration of vacancies on the Li(1) sites.[10] Later, Isasi et al.[15,16] reported various structures for similar compounds $Li_5Ln_3M_2O_{12}$, where M = Sb and Ln = La, Pr, Nd, Sm as isostructural with the Hyooma model, but with partial occupancies $^5/_6$ for both Li sites. For further discussion of the structure models it should be kept in mind that the space group $I2_13$ assumed in the Hyooma model is not the maximal subgroup of the ideal garnet space group $Ia\bar{3}d$; the symmetry reduction is at least formally a two-step process which may run either via space group $Ia\bar{3}$ (No. 206) or via $I4_132$ (No. 214), which thereby appear to be further candidates for an appropriate description of the compound.

In the present study, we have employed the bond valence mismatch calculation study to control the chemical plausibility of the published structure models and to identify probable pathways for Li^+ ionic motion in $Li_5La_3M_2O_{12}$. Our results show that the characteristic feature of the three-dimensional Li-pathway network is a nonplanar square of Li positions.

2. Experimental Aspects

Compounds with the chemical formula $Li_5La_3M_2O_{12}$ (M = Nb, Ta) were prepared by solid-state reaction using appropriate amounts of $La(NO_3)_3 \cdot 6H_2O$ or La_2O_3 (heated at 900 °C for at least 24 h), $LiOH \cdot H_2O$, and M_2O_5 (M = Nb, Ta) by reacting them at 700 °C for 6 h and 900 °C for 24 h in air. Then 10 wt % excess of $LiOH \cdot H_2O$ was added to compensate for the loss of lithium due to evaporation at elevated temperatures. After each stage of heat treatment, the powders were ball-milled using zirconia balls for 12 h in 2-propanol. At the final stage of heat treatment, the reaction products were pressed into pellets by isostatic pressure and the pellets were covered with the same powder to decrease the loss of lithium due to evaporation. Powder X-ray diffraction (XRD, SEIFERT 3000, Cu Kα) was employed at room temperature to monitor the phase formation after each sintering step. Lattice constants were obtained by least-squares refinement of the powder XRD data using GSAS software.[17]

3. Bond Valence Analysis of Ion Transport Pathways

The bond valence method had originally been developed to assess equilibrium positions of atoms in crystal structures by means of the empirical relationship between bond length R_{A-X} and bond valence

$$s_{A-X} = \exp[(R_0 - R_{A-X})/b] \quad (1)$$

(where R_0 and b represent empirical parameters) as sites where the sum of all individual interactions, the bond valence sum,

$$V(A) = \sum_X s_{A-X} \quad (2)$$

approaches the formal valence V_{ideal} (oxidation state) of the central atom A. As the bond valence sum (BVS) should match the absolute value of the oxidation state V_{ideal} for each atom in the crystal structure of a thermodynamically stable phase, BVS calculations are widely used to assess the chemical plausibility of suggested crystal structures. Salinas-Sanchez[18] suggested to quantify the plausibility of a structure by the so-called "global instability index (GII)"

(13) Wells, A. F. *Structural Inorganic Chemistry*, Fifth Edition; Clarendon Press: Oxford, 1984.
(14) Wyckoff, R. W. G. *Crystal Structures: Inorganic Compounds $R_x(MX_4)_y$, $R_x(M_nX_p)_y$, Hydrates and Ammoniates*, 2nd ed.; Interscience Publishers: New York, 1960; Vol. 3.
(15) Isasi, J.; Veiga; M. L.; Jerez, A.; Pico, C. *J. Less-Common Met.* **1991**, *167*, 381.
(16) Isasi, J.; Veiga, M. L.; Saez-Puche, R.; Jerez, A.; Pico, C. *J. Alloys Compd*. **1991**, *177*, 251.
(17) Larson, A. C.; Von Dreele, R. B. General Structure Analysis System (GSAS); Report LAUR 86-748; Los Alamos National Laboratory: Los Alamos, NM, 2000.
(18) Salinas-Sanchez, A.; Garcia-Munoz, J. L.; Rodriguez-Carvajal, J.; Saez-Puche, R.; Martinez, J. L. *J. Solid State Chem*. **1992**, *100*, 201.

$$\mathrm{GII} = \sqrt{\frac{\sum_{A=1}^{N}[V(A) - V_{\mathrm{ideal}}(A)]^2}{N}} \qquad (3)$$

that is, the root-mean-square average mismatch of the BVS for each of the N crystallographically distinct atoms A within the unit cell. A GII value >0.2 is typically taken as an indication that there is a problem with the reported structure model.[19]

The analogous postulate that the BVS of a mobile ion A^+ tends to match the oxidation state not only for equilibrium sites but also for any site that the ion accesses along its pathway straightforwardly leads to models of ion transport pathways in solid electrolytes: low-energy transport pathways for the motion of ions between equilibrium sites should correspond to pathways along which the BVS mismatch $\Delta V(A) = |V(A) - V_{\mathrm{ideal}}(A)|$ for A^+ remains as low as possible.

Peculiarities of the particular bonding type of each kind of atom pair are expressed by the values of the empirical parameters R_0 and b. Thus, covalent and ionic bonding may be treated by a common formalism and the terms "anion" and "cation" refer only to the relative electronegativity of the particles. The most widely employed tables of empirical bond valence parameters are based on the postulate that $V(A)$ is completely determined by interactions of A to counterions in its first coordination shell. Since the limited range of bond lengths in this first coordination shell obstructs an independent refinement of R_0 and b in eq 1 from reference crystal structures, Brown and Altermatt[19] had suggested to use a universally fixed value of $b = 0.37$ Å and to refine only R_0. The key effect of this simplification and the pseudopotential-type nature of the bond valence approach become evident by rewriting the monotonic decrease of the bond valence s_{A-X} with increasing bond length R_{A-X} in eq 1 into the bond valence mismatch

$$\Delta s_{A-X} = \left|\exp\left[\frac{R_0 - R_{A-X}}{b}\right] - s_{\mathrm{ideal}}\right| \qquad (4)$$

caused by varying the length of a single $A-X$ bond in the coordination shell of A. For a given value of s_{ideal} (i.e., for given values of the formal cation charge and the coordination number) the shape of this pseudopotential depends only on the value of b. The postulate of a universally fixed value of b thereby would, for example, enforce an identical shape of the bond valence mismatch "potential" for all monovalent cations in octahedral coordinations, irrespective of the polarizability of the interacting atoms. Applications of bond valence calculations to nonequilibrium sites require more realistic estimates of the relationship between bond length and bond valence mismatch and hence an adaptation of b to the "softness" of the bond for the specific atom pair.

In the frame of our effort to establish a consistent set of bond softness sensitive bond valence parameters (softBV), we have recently studied bond length bond valence correlations in alkali chalcogenides and alkali halides[20] and in particular for Li−O bonds. We could demonstrate that the significance of the refinement of b values from well-determined fully ordered reference crystal structures (extracted from the ICSD structure database[21]) can be notably enhanced by taking into account the weak interactions to more distant counterions. This also permitted derivation of a general quantification of the relationship between bond softness and bond valence parameters based on Parr and Pearson's[22,23] "absolute softness" σ as an independent measure of the particle softness.[20,24] Obviously, atom combinations with flatter potentials (corresponding to higher values of b) result in lower valence mismatch barriers for moving ions and therefore favor ion mobility in solid electrolytes. As expected, the softBV parameter b(Li−O) is significantly higher than that for the interaction of other alkali cations with oxide anions.

Bond valence models of Li^+ transport pathways are then constructed by calculating the BVS that a hypothetical Li^+ ion would feel at each site of a dense three-dimensional (3D) grid covering the entire local structure model. Connections between equilibrium sites, along which the valence mismatch remains as low as possible,[25−27] should then reproduce pathways along which an ion transport would require the lowest possible activation energy. Vivid graphical representations of the transport pathways can be accomplished by drawing 3D isosurfaces of constant BVS mismatch within the structure model. For low threshold values of ΔV(Li) these isosurfaces normally show isolated equilibrium sites (as well as low-energy interstitial sites if these exist). For higher threshold values the isosurfaces will include regions that the mobile ions can reach from the equilibrium sites with an activation energy that corresponds to ΔV(Li). Continuous paths for long-range ionic motion and hence for dc ionic conductivity can be located by increasing the threshold until the pathways become infinite. Of course, it has to be checked additionally that these infinite pathways include both occupied and vacant sites.

For crystal structures with a moderate degree of disorder in the immobile sublattice the average structure should be sufficiently close to a characteristic local structure and the bond valence analysis can be applied directly to crystal structure data, whereas for highly disordered or amorphous materials the information extracted from diffraction studies needs to be translated into models of characteristic local environments for the mobile ions with the help of molecular dynamics simulations or reverse Monte Carlo fits.[26−29] In the case of Ag^+ ion conductors, where independent models of conduction pathways can be derived from a detailed analysis of single-crystal diffraction data in terms of

(19) (a) Brown, I. D. *The chemical bond in inorganic chemistry: the bond valence model* (International Union of Crystallography monographs on crystallography; 12); Oxford University Press: Oxford, 2002. (b) Brown, I. D.; Altermatt, D. *Acta Crystallogr. B* **1985**, *41*, 244.

(20) Adams, S. *Acta Crystallogr. B* **2001**, *57*, 278.

(21) Inorganic Crystal Structure Database (ICSD), FIZ Karlsruhe, Germany, 1998.

(22) Parr, R. G.; Pearson, R. G. *J. Am. Chem. Soc.* **1983**, *105*, 1503.

(23) Pearson, R. G. *Inorg. Chem.* **1988**, *27*, 734.

(24) Adams, S. softBV; University of Göttingen: Göttingen, Germany, 2003; http://kristall.uni-mki.gwdg.de/softBV/.

(25) Garrett, J. D.; Greedan, J. E.; Faggiani, R.; Carbotte, S.; Brown, I. D. *J. Solid State Chem.* **1982**, *42*, 183.

(26) Adams, S. *Solid State Ionics* **2000**, *136/137*, 1351.

(27) Adams, S.; Swenson, J. *Solid State Ionics* **2002**, *154/155*, 151.

(28) Adams, S.; Swenson, J. *Phys. Rev. Lett.* **2000**, *84*, 4144.

(29) Adams, S.; Swenson, J. *Phys. Rev. B* **2001**, *63*, 054201.

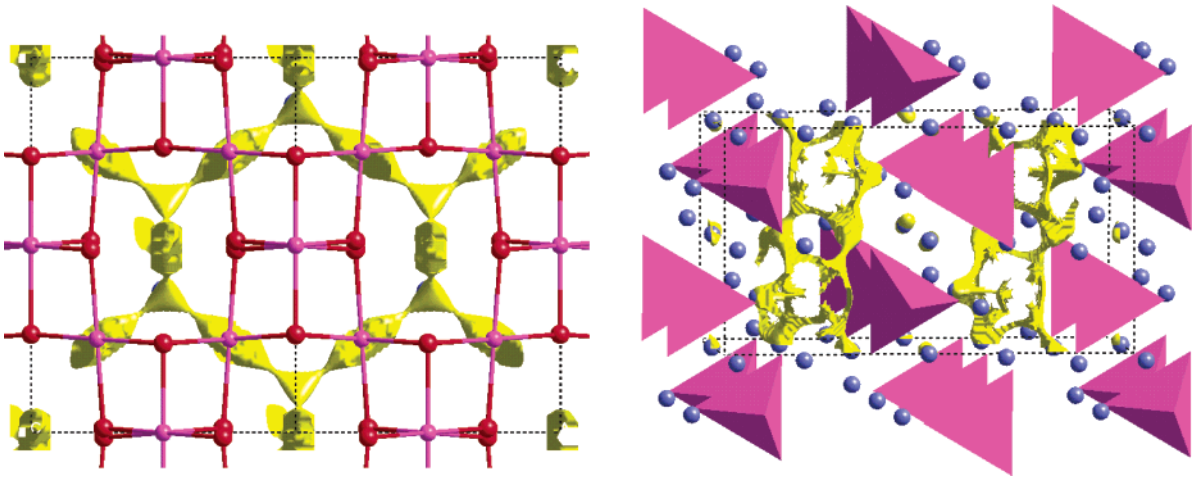

Figure 1. Bond valence model of infinite Li^+ transport pathways in spinel-type $LiMn_2O_4$ (left-hand side: O, red; Mn, magenta) and the thio-LISICON Li_4GeS_4 (right-hand side: Li, blue; GeS_4 shown as tetrahedra) represented by (yellow) isosurfaces enclosing regions of sufficiently small Li bond valence sum mismatch.

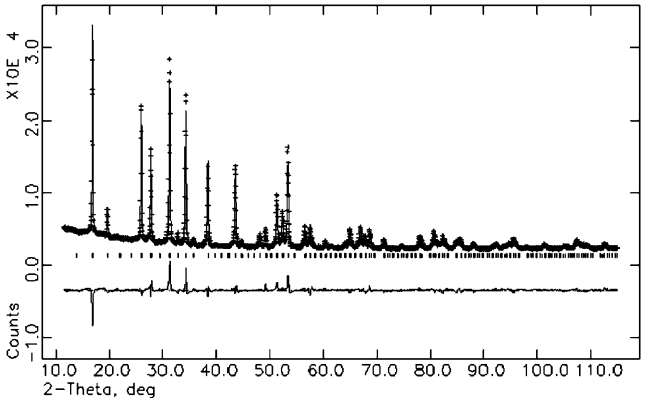

Figure 2. Rietveld fit for $Li_5La_3Nb_2O_{12}$ powder data assuming the structure model by Hyooma and Hayashi.[12]

anharmonic atomic displacement parameters, previous studies had demonstrated that the experimentally observed pathways closely match the predictions from bond valence methods.[26,27] For Li^+ conductors a direct pathway determination from diffraction data is hardly possible, while the bond valence prediction of Li^+ pathways requires only the knowledge of the immobile substructure and thus remains applicable. As typical examples, Figure 1 displays the infinite network of Li^+ pathways in spinel-type lithium manganate, a well-known lithium battery electrode,[30] and the prototype of the thio-LISICON compounds Li_4GeS_4.[31]

4. Results and Discussion

4.1. Crystal Structures. Powder XRD data for both $Li_5La_3Nb_2O_{12}$ and $Li_5La_3Ta_2O_{12}$ confirm the formation of a single phase with a garnet-like structure.[11,12] The lattice constants obtained from Rietveld fits are 12.826 and 12.829 Å for $Li_5La_3Nb_2O_{12}$ and $Li_5La_3Ta_2O_{12}$, respectively. Figure 2 shows the Rietveld refinement of powder XRD data for $Li_5La_3Nb_2O_{12}$ using the single-crystal structure data as starting atomic coordinates. Further insight into structural details from the Rietveld refinements is limited as the small structural differences affect the quality of the fit only marginally and it is not clear whether the slightly better fit achieved using the $I2_13$ model could be an artifact due to the much higher number of adjustable parameters. Only neutron diffraction data could provide a direct experimental access to the oxide ion arrangement, but even then a conclusive result about the lithium distribution appears questionable.

4.2. Global Instability Index (GII) Values. A closer look at the structures still reveals that both published models[11,12] are probably not highly precise as they are characterized by comparatively high values of the global instability index. For $Li_5La_3Nb_2O_{12}$ (that will be used as the example) a plausibility check using the softBV parameters yields GII = 0.31 valence units (v.u.) for the Mazza model[11] and GII = 0.22 v.u. for the Hyooma model,[12] if we employ identical lattice constants from our Rietveld refinement to exclude the effect of the lattice constants on the GII. The corresponding GII values for $Li_5La_3Ta_2O_{12}$ are 0.24 and 0.28 v.u., respectively. Moreover, the Mazza model leads to a distance <2.3 Å between La and the octahedrally coordinated Li site, which is ca. 0.6 Å shorter than a realistic minimum La−Li distance. Such unfavorable close cation contacts are only avoidable in a structure model that exhibits (at least locally) a lower symmetry. Finally, we could identify a single Bragg peak at $2\Theta \approx 41°$ (530 or 433) from our XRD powder patterns with extremely long measurement time (100 s/step) which unambiguously violates the extinction rules of the SG $Ia\bar{3}d$, while the same peak is permitted both in $I2_13$ and in the two intermediate space groups $I4_132$ and $Ia\bar{3}$ (as 433).

As a next step, we checked whether the structure model proposed by Hyooma might be as well-described with a lower number of free parameters in either $Ia\bar{3}$ or $I4_132$. It turned out that it is possible to describe the model equally well in the centrosymmetric supergroup $Ia\bar{3}$ after minute shifts of the published atomic parameters (shifts by 0.02 Å for La, 0.06−0.09 Å for oxygen, and 0.13 Å for the anyway ill-determined Li site to make pairs of atoms La1−La2, O1−O2, O3−O4, and Li1−Li2 congruent; for the Ta compound the required shifts are

(30) (a) Ammundsen, B.; Rozière, J.; Islam, M. S. *J. Phys. Chem. B* **1997**, *101*, 8156. (b) Lee, Y. J.; Wang, F.; Mukerjee, S.; McBreen, J.; Grey, C. P. *J. Electrochem. Soc.* **2000**, *147*, 803.

(31) Muruyama, M., Kanno, R. Kawamoto, Y., Kamiyama, T. *Solid State Ionics* **2002**, *154−155*, 789.

Table 1. Bond Valence Optimized Structure Model for $Li_5La_3Nb_2O_{12}$ in the Cubic Space Group $Ia\bar{3}$

(A) Fractional Coordinates[a]

atom	site	*x*	*y*	*z*	occupancy
La	24d	0.1264	0	1/4	1
Nb(1)	8a	0	0	0	1
Nb(2)	8b	1/4	1/4	1/4	1
Li	48e	0.6318	0.3244	0.5814	5/6
O(1)	48e	0.2802	0.1012	0.2260	1
O(2)	48e	0.3637	0.5264	0.4346	1

(B) Bond Lengths (in Å), Individual Bond Valences *s* (in v.u.) of the First Coordination Shell, and Bond Valence Sums *V* (in v.u.)[b]

La	−O(1):	2 × 2.3819 *s* = 0.494	
		2 × 2.9419 *s* = 0.143	
	−O(2):	2 × 2.3950 *s* = 0.480	
		2 × 2.5829 *s* = 0.316	*V* = 2.994
Nb(1)	−O(2):	6 × 1.9680 *s* = 0.815	*V* = 5.002
Nb(2)	−O(1):	6 × 1.9715 *s* = 0.809	*V* = 5.004
Li	−O(1):	1.9286 *s* = 0.230	
		1.9262 *s* = 0.231	
		2.6952 *s* = 0.052	
	−O(2):	2.6746 *s* = 0.054	
		2.6541 *s* = 0.057	
		1.9262 *s* = 0.231	*V* = 0.934
O(1)	−Nb(2):	1.9715 *s* = 0.809	
	−La:	2.3819 *s* = 0.494	
		2.9419 *s* = 0.143	
	−Li:	1.9286 *s* = 0.192	
		2.6952 *s* = 0.043	
		1.9261 *s* = 0.193	*V* = 1.966
O(2)	−Nb(1):	1.9680 *s* = 0.815	
	−La:	2.3950 *s* = 0.480	
		2.5829 *s* = 0.316	
	−Li:	2.6746 *s* = 0.045	
		2.6541 *s* = 0.047	
		1.9262 *s* = 0.193	*V* = 1.977
			GII = 0.0319 v.u.

[a] Lattice constant $a = 12.826$ Å. [b] Bond valence sums include further weak contributions from the second coordination shell.

in the same order of magnitude 0.02−0.13 Å), while a description in $I4_132$ would require significantly larger atomic rearrangements. The additional symmetry center relating the Li1 and Li2 site of the Hyooma model automatically implies that their occupancies are identical ($n = 5/6$). Although the number of refinable atomic coordinates is thereby reduced from 20 to 10, this model describes our XRD data equally well (yielding an even slightly lower $R(F^2) = 0.087$ instead of 0.091 for the Hyooma model for the Nb compound) and is characterized by an only marginally higher GII = 0.24 v.u. The nearest Li−La distance is slightly reduced by this averaging of the Li site to $x = 0.12495$ so that we preferred to retain the value $x = 0.1264$ for La(1) from the Hyooma model in harmony to both our Rietveld refinement and a slight reduction of GII.

4.3. Adjustment of Light Atom Positions by Optimization of the GII Value. Since the precision in the determination of atomic positions from X-ray data is generally much lower for the light atoms oxygen and lithium (particularly in the neighborhood of heavier atoms), it appears possible to enhance the plausibility of the structure model by an optimization procedure that minimizes the GII value by slightly varying the positions of the O and Li atoms, keeping the positions of the heavy atoms (La, Nb, or Ta) fixed. The optimization procedure of course needs to ensure that minimum cation−cation and anion−anion distances are respected and that individual bond valences should not be larger than appropriate for a single bond. Since all minimization algorithms are prone to lead to local minima, the GII minimization has to be repeated frequently. As the number of conceivable local minima steeply rises with the number of parameters that are to be optimized, it is not surprising that the most satisfactory structure model with GII = 0.032 v.u. was found by minimizations in the centrosymmetric space group $Ia\bar{3}$ (for details see Table 1 and Figure 3b), although the same atomic arrangement can of course be expressed in any lower symmetry. In this structure model all Li ions occupy

Table 2. Comparison of Bond Valence Light Atom (Oxygen and Lithium) Optimized Atomic Coordinates in SG $I2_13$ for $Li_5La_3M_2O_{12}$ (M = Nb, Ta) with Original[12] Single-Crystal Data[a]

	$Li_5La_3Nb_2O_{12}$				$Li_5La_3Ta_2O_{12}$			
atom	*x*	*y*	*z*	V^b/v.u.	*x*	*y*	*z*	V^b/v.u.
La1	0.1264(1)	0	0.25	2.907	0.1267(1)	0	0.25	2.898
				2.985				*2.985*
La2	−0.1235(1)	0	−0.25	2.856	−0.1214(1)	0	−0.25	2.922
				3.008				*2.991*
M1	0	0	0	5.256	0	0	0	4.737
				5.006				*5.011*
M2	0.25	0.25	0.25	4.566	0.25	0.25	0.25	4.309
				5.011				*5.001*
O1	0.2793(4)	0.1024(4)	0.2989(4)	1.797	0.2792(7)	0.0989(7)	0.2033(7)	1.769
	0.2758	*0.1073*	*0.1956*	*1.947*	*0.2747*	*0.1115*	*0.2002*	*1.965*
O2	−0.2830(6)	−0.1074(6)	0.3049(6)	1.770	−0.2853(7)	−0.1075(7)	−0.1921(7)	1.733
	−0.2795	*−0.1113*	*−0.1943*	*1.956*	*−0.2731*	*−0.1075*	*−0.1855*	*1.961*
O3	0.3576(6)	0.5284(6)	0.440(6)	2.068	0.3592(7)	0.5292(7)	0.4444(7)	1.951
	0.3623	*0.5322*	*0.4362*	*1.953*	*0.3639*	*0.5379*	*0.4494*	*1.938*
O4	−0.3543(4)	−0.5317(4)	−0.4492(4)	1.849	−0.3539(7)	−0.5318(7)	−0.4517(7)	1.846
	−0.3595	*−0.5290*	*−0.4497*	*1.930*	*−0.3535*	*−0.5274*	*−0.4509*	*1.926*
Li1	0.6036	0.3074	0.5331	0.762	0.6030	0.3070	0.5330	0.796
	0.6238	*0.3264*	*0.5797*	*0.843*	*0.6219*	*0.3301*	*0.5760*	*0.834*
Li2	−0.6175	−0.3033	−0.5461	0.821	−0.6170	−0.3010	−0.5460	0.842
	−0.6224	*−0.3219*	*−0.5477*	*0.889*	*−0.6076*	*−0.3209*	*−0.5800*	*0.909*
GII[b]				0.222				0.280
				0.070				*0.070*

[a] GII-optimized coordinates and bond valence sums are shown in italics. In comparison to the original data[12] the coordinates for several atoms have been replaced by their symmetry equivalents to illustrate the proximity of this model to the centrosymmetric description chosen in Table 1. All sites are fully occupied except Li(1), where the occupancy value is fixed at 2/3. [b] Bond valence sums and GII for lattice constants from GSAS refinement 11.826 Å (for M = Nb) and 11.829 Å (for M = Ta). GII values 0.211 (M = Nb) and 0.260 (M = Ta) result for the original lattice constants and atomic coordinates from ref 12.

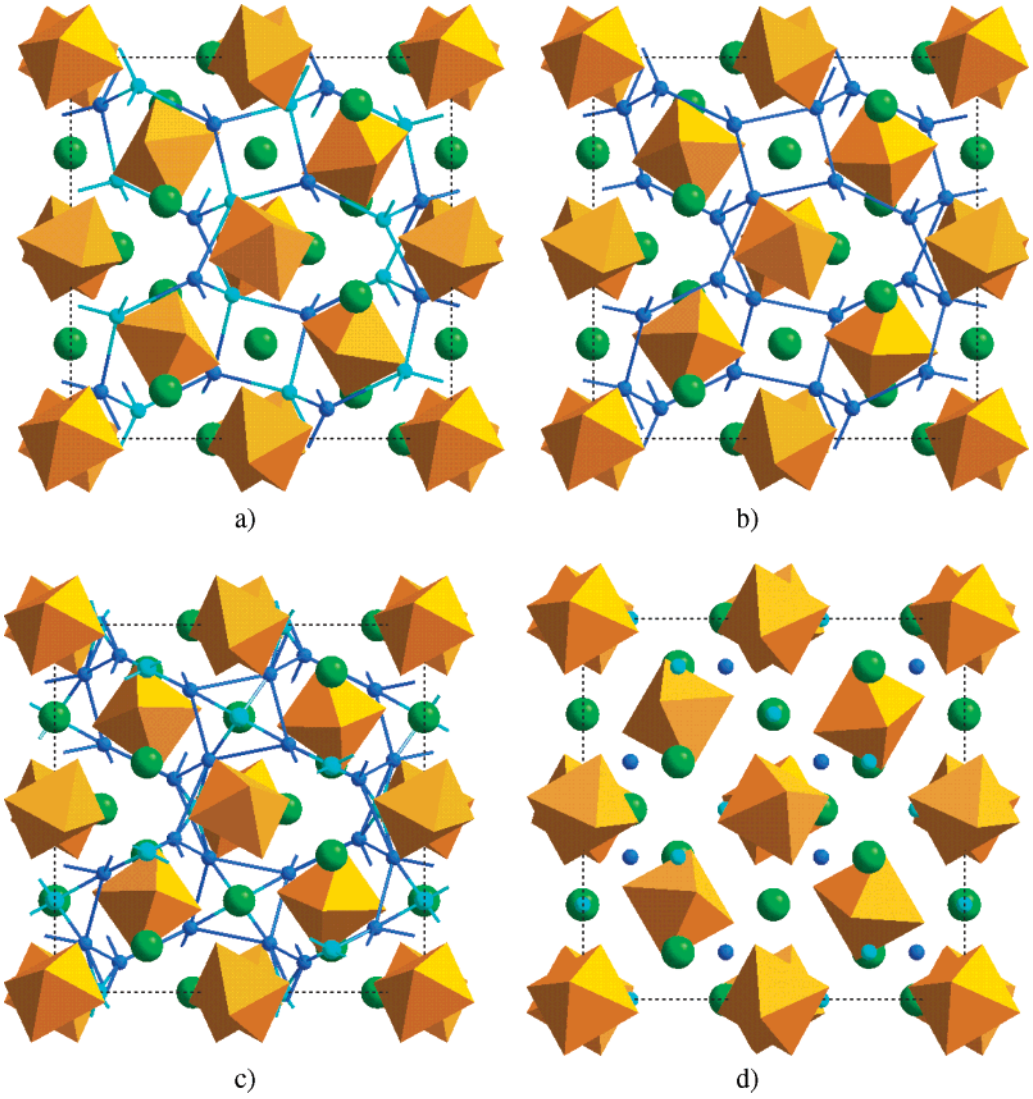

Figure 3. Alternative structure models for $Li_5La_3Nb_2O_{12}$ (NbO_6, orange octahedra; La, large green spheres; crystallographically distinct Li sites are marked by light and dark blue small spheres). The network of Li sites is sketched by connecting lines between adjacent Li sites. (a) In SG $I2_13$ after Hyooma and Hayashi:[12] 40 Li distributed on two distinct 24-fold octahedral sites (one of them fully occupied); (b) in SG $Ia\bar{3}$ assuming that the 40 Li occupy one distorted 48-fold octahedral Li site or (c) in SG $Ia\bar{3}$ assuming that besides the 48-fold Li site a small fraction of the Li occupies a 24-fold Li site with a distorted tetrahedral coordination. (d) For comparison the less plausible $Ia\bar{3}d$ model after Mazza[11] is also included, which assumes a Li distribution on a 24-fold octahedral site and a 16-fold tetrahedral site so that both sites would be fully occupied. This model will not be discussed further. To reduce the overlap, only half of the unit cell is shown along the *x*-axis (perpendicular to the plane). In the cases (b)−(d) the displayed positions of the light atoms Li and O are GII-optimized.

the same strongly distorted octahedral site (3 + 3 coordination) with an occupancy of $^5/_6$. Starting directly from the Hyooma model (Figure 3a), the lowest GII that we achieved for fixed Li occupancies in SG $I2_13$ was only 0.07 v.u. (for details see Table 2). The corresponding optimizations for the Ta compound lead to essentially the same minima (GII = 0.070 v.u. in $I2_13$ and 0.0323 v.u. in $Ia\bar{3}$) as illustrated in Tables 2 and 3 .

As the Mazza model suggests that a part of the Li ions resides on the tetrahedral sites (i.e., the Si sites of the ideal garnet structure), we also tested this possibility. While fully occupied 24 tetrahedral *x*, 0, $^1/_4$ sites (with $x \approx {}^3/_8$) would be incompatible with an occupancy of the four neighboring distorted octahedral sites (at a distance of ca. 2.0 Å), a partial occupancy of the surrounding octahedral sites leaves the possibility that, for example, 4 Li reside on the 24d tetrahedral site ($n = {}^1/_6$) and only 36 Li occupy $^3/_4$ of the "octahedral" 48e sites (cf. Figure 3c). A higher occupancy of the tetrahedral sites would require an ordering of the vacancies on the octahedral sites and thereby trigger a further symmetry reduction. A model with this Li distribution onto two sites leads to practically the same GII = 0.032 and almost the same structure model except for the additional distorted tetrahedral Li site (at $x = 0.383$). The Li distributions in the different structure models

Table 3. Bond Valence Optimized Structure Model for $Li_5La_3Ta_2O_{12}$ in the Cubic Space Group $Ia\bar{3}$[a]

atom	site	*x*	*y*	*z*	occupancy	*V*/v.u.
La	24d	0.1267	0	$^1/_4$	1	2.997
Ta(1)	8a	0	0	0	1	5.000
Ta(2)	8b	$^1/_4$	$^1/_4$	$^1/_4$	1	5.003
Li	48e	0.6312	0.3237	0.5824	$^5/_6$	0.933
O(1)	48e	0.2795	0.1011	0.2267	1	1.980
O(2)	48e	0.3639	0.5273	0.4349	1	1.963
						GII = 0.0323 v.u.

[a] Lattice constant $a = 12.829$ Å.

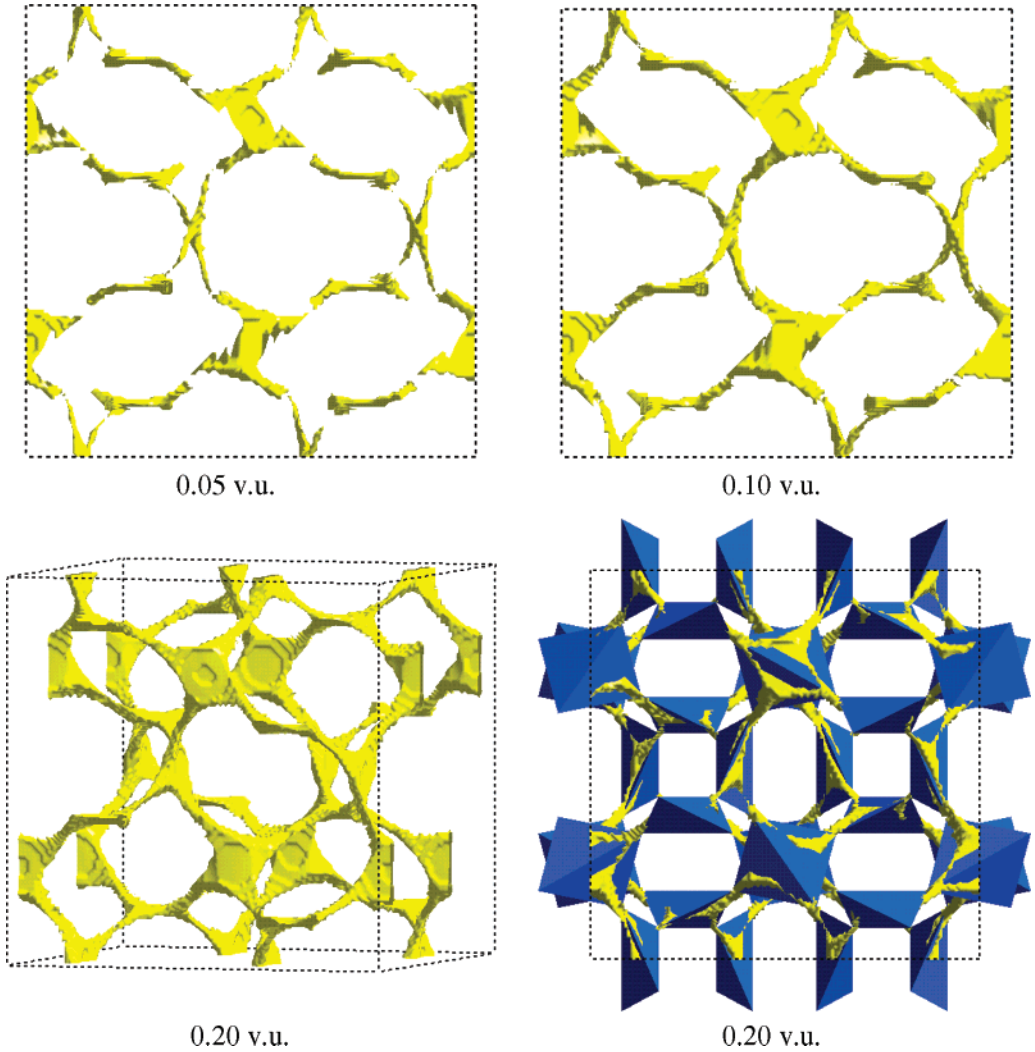

Figure 4. Isosurfaces of constant Li bond valence sum mismatch ΔV(Li) as models for Li^+-ion transport pathways in the GII-optimized structure model (c) in $Li_5La_3Nb_2O_{12}$. The isosurface for ΔV(Li) = 0.05 v.u. consists only of pathways for localized low-energy hops, while a continuous network of pathways exists only for ΔV(Li) ≥ 0.1 v.u. (As in Figure 3, the upper graphs show only half of the unit cell $0 < x < 1/2$). The BV model of the 3D network of Li^+-ion transport pathways (displayed on the lower left-hand side for the whole unit cell and ΔV(Li) = 0.2 v.u.) closely follows the network of Li site polyhedra (lower right-hand side). The center of each polyhedron is formed by a tetrahedral Li site, while the adjacent octahedral sites constitute the corners of the polyhedron.

are summarized in Figure 3. Both BVS optimized models in $Ia\bar{3}$ and the Hyooma model[12] will be used in the next section to analyze the Li transport pathways in the Nb compound in detail.

4.4. Conduction Pathways. Li^+-ion transport pathways in the above-mentioned structure models have been modeled as isosurfaces of constant Li^+ BVS mismatch. As the actually occupied Li sites do not directly affect these calculations, it is not too surprising that the results for the two GII-optimized models in $Ia\bar{3}$ (models (b) and (c) in Figure 3) are practically indistinguishable. Figure 4 displays isosurfaces for different threshold values of the constant Li BVS mismatch in the GII-optimized model (c) with two Li sites. Only for the lowest mismatch threshold 0.05 v.u. the isosurfaces are split into localized regions that span from the tetrahedral site (nearly) to the "octahedral site". For 0.1 v.u. the isosurface represents an infinite pathway for long-range ionic conduction that includes all fractionally occupied Li sites. A further increase of the BVS mismatch threshold does not reveal any additional interstitial sites or pathways for Li-ion migration.

While the two upper two graphs in Figure 4 illustrate the pathways (as Figure 3 the structures) only for one-half of the unit cell to reduce the overlap between pathways in different regions of the unit cell, the 3D character of the pathway network that is essential for a high conductivity under working conditions becomes obvious from the lower two figures. The pathway network essentially consists of nonplanar squares formed by the octahedral Li sites with an (almost) vacant tetrahedral site at the center. As the octahedral Li site belongs to two corner-sharing squares, a mobile Li at the equilibrium site has the choice between 4 neighboring equivalent Li sites (plus two tetrahedral sites) as potential target sites for an ion hop. Assuming a statistical distribution of the Li on the available sites, the probability that one of these target sites is unoccupied is >50% (even if tetrahedral sites are excluded as jump targets).

The Li network may alternatively be described as consisting of eight separate nearly planar hexagons of Li sites per unit cell, where each edge of a hexagon is connected to an edge of a different hexagon via the

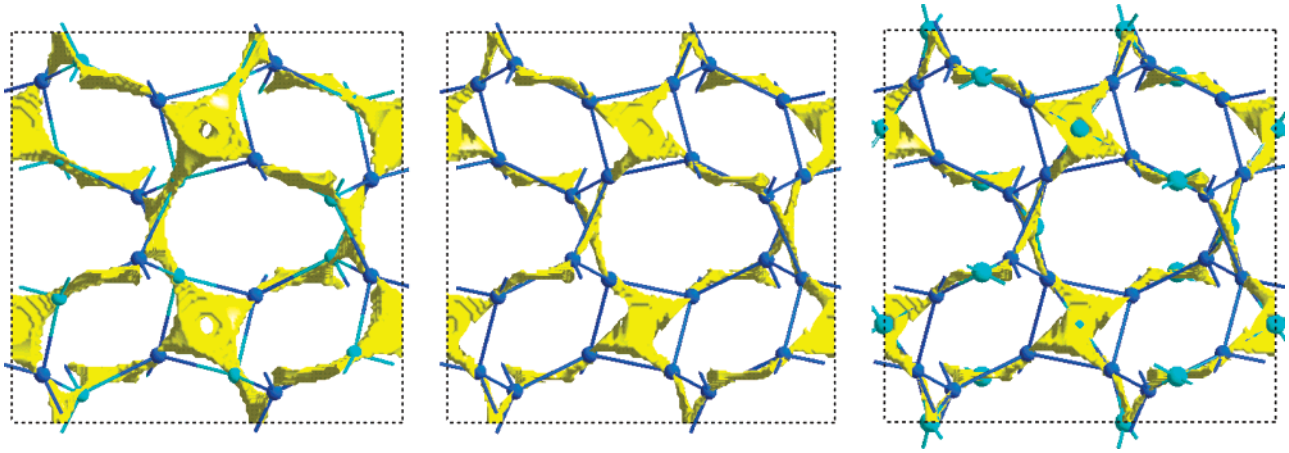

Figure 5. Comparison of bond valence models for Li^+ transport pathways in $Li_5La_3Nb_2O_{12}$ in the GII-optimized models (a)−(c) for $\Delta V(Li) = 0.1$ v. u. together with the respective network of partially occupied Li sites.

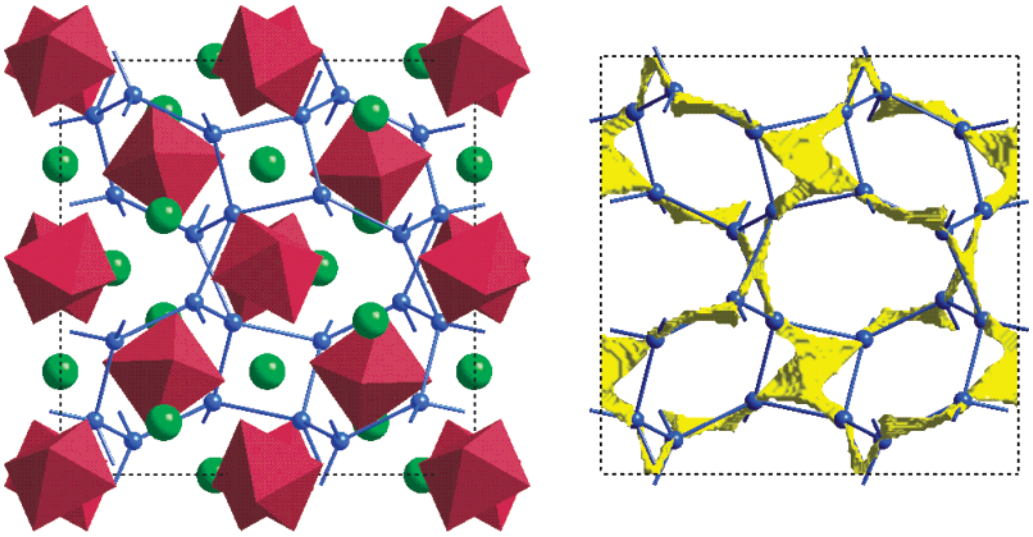

Figure 6. GII-optimized structure model of $Li_5La_3Ta_2O_{12}$ in $Ia\bar{3}$ (left-hand side) and bond valence model of Li^+ transport pathways (isosurface for $\Delta V(Li) = 0.1$ v.u.). Only half of the unit cell is shown along the *x*-axis.

above-mentioned "squares" (cf. Figures 3 and 5). The different orientations of the squares related to a single Li site hexagon ensure that each hexagon is connected to six different neighboring hexagons.

As demonstrated in Figure 5, bond valence pathway models for the different structure models (a)−(c) largely agree in the predicted Li^+ conduction pathways. Model (a) based on the structure reported by Hyooma and Hayashi contains almost the same extended region of low bond valence mismatch (that contains $^{10}/_3$ Li^+ ions) within each nonplanar square of octahedral sites as the centrosymmetric models (b) and (c). The low (or even zero) occupancy of the tetrahedral site can be traced back to a repulsive interaction with a neighboring La^{3+}.

Figure 6 displays the Li^+ transport pathway models for $Li_5La_3Ta_2O_{12}$ based on the $Ia\bar{3}$ structure model (b) (cf. Table 3). As expected, pathways are nearly identical to those for $Li_5La_3Nb_2O_{12}$ and will therefore not be discussed in detail. Due to the simplicity of the bond valence approach, it appears questionable whether the minute structural differences (e.g., in the tilt angle of the MO_6 octahedron) should be considered as significant. ^{7}Li NMR investigations of $Li_5La_3Nb_2O_{12}$ and $Li_5La_3Ta_2O_{12}$ are currently in progress to elucidate further details of the Li^+-ion transport mechanism on the basis of the present pathway analysis.

The bond valence models consistently suggest that the Li^+-ion transport pathways in $Li_5La_3Nb_2O_{12}$ and $Li_5La_3Ta_2O_{12}$ directly connect the almost fully occupied octahedral sites. Thus, a vacancy type ion transport is expected to be the dominant contribution to the long-range ion transport, while the tetrahedrally coordinated "interstitial sites" mainly act as sources or sinks of mobile ions. Besides increasing the number of vacancies, this may also lead to an interstitialcy type contribution to the Li^+ conductivity. There is, however, no indication of a pathway connecting interstitial sites as would be necessary for an interstitial mechanism.

While the transport properties of glassy solid electrolytes can be predicted by means of a bond valence analysis from models of their instantaneous local structure,[27−29] the experimental activation energy ΔE (or more precisely the activation energy of the decisive elementary process) of crystalline solid electrolytes can so far only be roughly assessed from the threshold value of the valence mismatch ΔV necessary to create infinite pathways. Besides ΔV this estimate depends both on the mass and the degree of ordering of the mobile ions. As discussed more in detail elsewhere,[32] a steep slope of the $\Delta E(\Delta V)$ correlation results for compounds with

(32) Adams, S.; Swenson, J. Submitted to *Solid State Ionics*.

structural disorder of the light mobile ion Li^+. Thus, both experimentally observed activation energies (0.43 eV for the Nb compound and 0.56 eV for the Ta compound)[10] appear to be compatible with the prediction 0.5 eV from the nearly identical threshold value of ΔV. When discussing minor differences between the properties of the investigated compounds, it should also be kept in mind that the experimental determination of precise activation energies is nontrivial in these cases because of the variability of the stoichiometry and its effect on cation oxidation states, lattice constants, local ordering, etc.

It may be expected that a partial replacement of the La^{3+} by smaller size and/or lower valence cations will significantly affect the connectivity of the network by controlling the number of easily accessible vacancies and hence conductivity could be tailored further by appropriate chemical substitutions.

5. Concluding Remarks

The bond valence analysis of Li^+ distribution and ion transport pathways reveals the structural origin of the experimentally observed high ionic conductivity in the garnet-related structures $Li_5La_3M_2O_{12}$ (M = Nb, Ta). The Li^+ ions move in a three-dimensional network of energetically equivalent partially occupied sites. The number of accessible equivalent Li^+ sites is not only 20% higher than the number of occupied sites. The additional possibility of complex Li^+ rearrangements in an extended region of low bond valence sum mismatch centered by a further (almost) vacant tetrahedrally coordinated Li site should further enhance the conductivity and underlines the potential of this new class of fast ion conductors.

Modifications of the compound to optimize the transport properties have to take into account the strong influence of the repulsive interaction between the large La^{3+} cations on the accessibility of this nearly quadratic flat core region of the pathways for mobile Li^+ ions.

Acknowledgment. One of us (V.T.) thanks the Deutscher Akademischer Austauschdienst (DAAD) for financial support.

CM031176D